Arch. Metall. Mater. **70** (2025), 2, 639-649

DOI: https://doi.org/10.24425/amm.2025.153465

TIJUN CHEN[1*], QINSONG HOU[1], YANGHUA LIU[1]

EFFECT OF ALLOY 2 COMPOSITION ON THE MICROSTRUCTURE OF Al-Si ALLOY PREPARED BY CONTROLLED DIFFUSION SOLIDIFICATION WITH SIMULTANEOUS MIXING

Taking pure Al as Alloy 1, the effect of Si content in Al-Si alloy (Alloy 2) on microstructures of Al-Si alloy castings prepared by controlled diffusion solidification with simultaneous mixing was investigated mainly by using theoretical simulation and calculation. The results indicate that at a given superheat, the Si content in the Al-Si alloy essentially affects the liquidus temperature, and thus, its mixing temperature and the temperature difference with pure Al melt, causing the variation of temperature field of the resulted mixture besides the solute field. As a result, both the supercooling degree and width of supercooling zone in the pure Al pockets are altered, and consequently the nucleation rate and the size and morphology of primary α-Al grains are varied. At the same liquidus and mixing temperatures (also the same temperature difference with the pure Al melt), the nucleation rates at using hypoeutectic Al-Si alloys are higher than those at using hypereutecitc ones due to the larger supercooling degree and width of supercooling zone of the former condition than the latter condition. Subsequent experiment results on microstructure observation of the CDS castings verify these results, and further confirm that an ideal nondendritic microstructure can be achieved only when the nucleation rate is up to a critical value (corresponding to 30% of solidified mesh number in the simulation).

Keywords: Controlled diffusion solidification; Al-Si alloy; Supercooling zone; Nucleation rate; Nondendritic grains

1. Introduction

Porosities in castings are the most common defect [1], and hot cracks in wrought alloy castings are the the biggest problem that hinders the wrought alloys to be well cast [2]. The essential for forming these two kinds of defect is all contributed to the dendritic solidification mode during casting [3]. Therefore, if the dendritic solidification mode is changed into a nondendritic way and a fine nondendritic (i.e., spheroidal) microstructure is achieved, these defects can be significantly decreased and even avoided. So far, there are two categories of processing technology that can reach this assumption, named semisolid forming (SSF) and controlled diffusion solidification (CDS), by which an integrated casting with compact nondendritic microstructure can be achieved [4,5].

For SSF, the required materials prior to forming must be a semisolid slurry (for rheoforming) or ingot (for thixoforming) with nondendritic primary particles that are uniformly suspended in liquid phase, and such materials need to be prepared in advance by using specific technologies [4]. Compared with the traditional casting technologies, the process of SSF is quite complicated, and thus, the production efficiency is relatively lower and the cost of products is higher. As to CDS, its process is quite simple, in which one precursor alloy melt (Alloy 1) with high thermal mass (high temperature and large mass) is poured into another precursor alloy melt (Alloy 2) with low thermal mass, and then the resulted mixture (Alloy 3) is immediately cast [5,6]. That is, only two extra crucibles for mixing and one mixing procedure are needed compared with the traditional casting technologies. So CDS is a more promising way for producing nondendritic castings.

The available investigations propose that the achieved mixture is composed of numerous small pockets of the two precursor melts, the marginal regions of Alloy 1 pockets are quickly cooled into a supercooling state by surrounding Alloy 2 melt, and thus, copious nucleation occur in these regions and then grow in a stable solid/liquid interface, which is resulted from the back diffusion of solutes in Alloy 2 melt toward the solid/liquid interface, just opposite to the conditions of conventional casting, resulting in forming a small and nondendritic-grained microstructure [5-7]. Namely, the copious nucleation and no constitutional supercooling in the liquid ahead of solid/liquid interface (when Alloy 1 is pure metal) are the sources for forming the small and nondendritic-grained microstructure [8].

[1] LANZHOU UNIVERSITY OF TECHNOLOGY, STATE KEY LABORATORY FOR ADVANCED PROCESSING AND RECYCLING OF NONFERROUS METALS, LANZHOU 730050, CHINA

* Corresponding author: chentj1971@126.com

Based on this mechanism, it can be expected that the number, size and distribution of Alloy 1 pockets, and their supercooling degrees closely influence the final casting microstructure, and they are determined by the mixing effect, and mass ratio and temperatures of the two precursor melts. For this purpose, the existing investigations give the main conditions for a successful CDS, such as the superheat degrees of the three melts (Alloy 1, 2 and 3) should be lower than 10 K and even the temperature of Alloy 3 is lower than its liquidus, the temperature of Alloy 1 is 50 K higher than that of Alloy 2, and the mass ratio of Alloy 1/Alloy 2 is higher than 3 [4-7]. As expected, some-composition alloys cannot be shaped by CDS due to the limitation of the requirement about mass ratio. More importantly, all the requirements are well matched, but abnormally large and irregular grains inevitably exist in the resultant castings [9]. In addition, the experiment results also show that a lower mixing ratio always results in a microstructure with smaller and more spheroidal primary grains [10], which must decrease the production efficiency of CDS. Essentially, the requirements about the large mass ratio and low mixing rate are for achieving a good mixing effect, and the abnormal grains are contributed to the undesirable mixing effect [8,11]. To improve the mixing effect and overcome the related shortcomings, the authors developed a modified CDS, named CDS with simultaneous mixing, in which two precursor melts were simultaneously poured in their respective pouring rates, the two melt streams first encountered in air and then fell into a mixing crucible, and finally the mixture was immediately cast (needing to ensure the pouring of the two precursor melts to simultaneously start and end) [12]. The experiment result by using 4/3 kg of pure Al, 8/3 kg of Al-12Si and 4 kg of Al-8Si alloys as Alloy 1, 2 and 3 respectively indicated that a casting with uniform microstructure (without abnormal grains) could be achieved, and the higher the mixing rate is, the smaller and more spheroidal the primary α-Al grains are. In this case, the mass ratio is 1:2, much smaller than the required 3:1 by the traditional CDS [4]. Namely, the modified CDS has more significant advantages than the traditional one [13].

As suggested, the modified CDS only affect the mixing effect and its essential is the same to that of the traditional one. The authors have investigated the mixing process, nucleation and growth mechanism, especially the effect of standing time after mixing on the mixture microstructure and the effect of mixing temperature on the microstructure of an Al-8Si during the modified CDS, through theoretical simulations and experiments [12-14]. The results more conclusively and intuitively confirmed the formation mechanism of the fine nondendritic microstructure mentioned above, the mixture should be poured as soon as possible (i.e., within 10 s) after mixing, and the mixing temperature should be low as possible (i.e., 5 K superheating degree or lower), in order to achieve small and spheroidal primary α-Al grains. Besides the above requirements, the absolute values of the three melts' Gibbs energies, the difference in surface tension of the two precursor melts, and the interface energy of solid/liquid have also been stipulated in some investigations [15,16]. It is expected that the compositions of the two precursor melts are the most important technological parameters of CDS, because their variations possibly lead to three aspects of change: (1) the liquidus temperatures of the two precursor melts, and thus, their mixing temperatures and the temperature difference between them, (2) the mass ratio at a given composition of Alloy 3 or the composition of Alloy 3 at a given mass ratio, and (3) the solute concentrations at front of advancing solid/liquid interface in Alloy 1 melt (when Alloy 1 is not a pure melt), and thus, the constitutional supercooling. Of course, their variations also cause the changes in Gibbs energy, surface tension and interface energy mentioned above. Namely, the changes in composition of precursor melts almost affect the satisfaction degrees with all the above requirements of CDS, consequently, the nucleation, growth mode and final morphology (size and shape) of primary grains in castings.

There have several reports to involve the CDS with different-composition precursor melts, but their concerns do not focus on the effect on nucleation, growth and morphology (size and shape) of primary grains. In an investigation from Khalaf et al., two-composition Alloy 2 melts (Al-4.7Cu and Al-7.7Cu, the compositions all refer to mass percentage (wt.%) unless otherwise stated) were referred, but the focus was concentrated to the formation of abnormal large grains [9]. In another report, also two-composition Alloy 2 melts (Al-12.6Si and Al-15Si), as well as two-composition Alloy 1 and Alloy 2 melts (Al-5.36Cu-0.88Fe-0.67Mg-3.9Si-0.88Zn (Alloy 1) with Al-13.5Si (Alloy 2), and Al-7.75Si-0.79Fe-0.78Zn-0.6 Mg (Alloy 1) with Al-24Cu (Alloy 2)) were concerned, and the effect of mixing ratio on the microstructure morphologies was primarily discussed [17]. Furthermore, a series of Al-Zn-Mg-Cu alloys with different solute concentrations was prepared by CDS using different-composition Alloy 1 and 2 melts, but the effects of eutectic phase fraction and secondary phase/precipitate amount on tensile properties of T4 and T6 heat treated alloys were mainly explored [18]. More importantly, other parameters such as superheat, mixing ratio and/or mixing rate of the precursor melts were also simultaneously altered besides the compositions of precursor melts as mentioned above. In this case, the unique effect of precursor melt composition on the microstructure of CDS casting is difficult to be clarified. Therefore, in this work, pure Al melt with a superheat of 5 K was taken as Alloy 1, 6-composition Al-Si melts with Si concentrations ranging from 7.2% to 15% and a superheat of 5 K were regarded as Alloy 2, and the mixing ratio was maintained at 1:2, the resultant temperature and solute fields in the mixture, nucleation status and conditions at solid/liquid interface were theoretically simulated and calculated, and then experiments were conducted to verify the theoretical results, in order to clarify the effect of Alloy 2 composition during CDS with simultaneous mixing.

2. Investigation methods

2.1. Simulation and calculation processes

It is quite difficult to clarify the mixing process of precursor melts, the microstructure, and the solute and temperature fields of

the resultant mixture during CDS by experimental way, theoretical simulation is thereby considered as a promising method [9,19]. Similar to the authors' previous investigations [12,13], Fluent software* was used to conduct the simulation, and the detailed method, process and mesh division were completely the same to those in reference [13]. For convenience, the schematic of the CDS process and dimensions of the used model are presented by Fig. 1. It is noted that the dimensions are half of those of the equipment used in the latter experiment in order to save the simulation time. As indicated above, pure Al was taken as Alloy 1 and Al-Si alloys with Si contents ranging from 7.2% to 15% were employed as Alloy 2. The values of thermophysical parameters of the two precursor melts are listed in TABLE 1, which were taken from the database of JMatPro software**. The meanings of all the involved symbols were also same as those in reference [15].

The CDS parameters employed in the simulation are given in TABLE 2. It can be found that the temperature (T_1) of pure Al (Alloy 1) melt was maintained at 938.15 K, i.e., the pure Al melt was superheated for 5 K, and those (T_2) of Al-Si alloy (Alloy 2) melts were varied with their compositions, but their superheats were also kept at 5 K (comparing with the corresponding liquidus temperatures in TABLE 1). The masses of the two precursor melts were always 1/3 (m_1) and 2/3 kg (m_2) respectively (i.e., the mass ratio was held at 1:2), and thus, 1 kg mixtures (Alloy 3) with Si content (C_3) from 4.8% to 10% were achieved after mixing. Correspondingly, the differences in temperature (ΔT) between the precursor melts changed within 45-80 K. The mixing rate was kept at a constant of 1 kg/s and the two precursor melts were simultaneously poured within 1 s at their respective pouring rates. Namely, the changes in composition and temperature of Alloy 2 simultaneously brought about the variations of temperature difference between the two precursor melts, and the composition (C_3) and liquidus temperature (T_{L3}) of Alloy 3, of course, the actual temperature (T_3) of Alloy 3 as listed in TABLE 2.

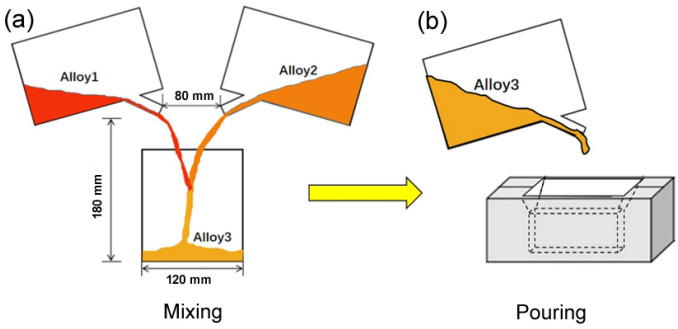

Fig. 1. Schematic of CDS process

Besides the temperature and solute fields achieved from the above simulation, the nucleation statuses at the different compositions of Alloy 2 were also analyzed based on the simulation results, and the method was same to that used in reference [13], that is, the number or percentage of solidified meshes was used to estimate the nucleus number or nucleation rate. Finally, to clarify the influence mechanism of the Alloy 2 composition on the nucleation status, and the growth mode, the conditions at solid/liquid interface were calculated and the detailed process was also described in reference [13]. It is known that nucleation needs time, and the time needed for forming a stable nucleus composed of many ordered atoms in a melt is approximately 10^{-8} s for most metals [20]. Thus, the conditions at the two melts contacting for 10^{-8} s were calculated.

TABLE 1

Thermophysical parameters of the two precursor melts used in simulation

Thermophysical parameters	Pure Al	Al-7.2Si	Al-8Si	Al-12Si	Al-13Si	Al-14.6Si	Al-15Si
T_L (K)	933.15	888.15	883.15	853.15	853.15	883.15	888.15
T (K)	938.15	893.15	888.15	858.15	858.15	888.15	893.15
ρ (g/cm^3)	2.394	2.435	2.442	2.461	2.463	2.466	2.467
C_p (J/g·K)	1.180	1.143	1.138	1.112	1.114	1.124	1.122
K_L (W/m·K)	90.16	83.03	82.24	78.46	77.73	77.37	77.23
μ (MPa/s)	1.29	1.56	1.59	1.82	1.83	1.72	1.70
D ($\times 10^{-9}$ m^2/s)	—	2.72	2.80	2.31	2.29	2.52	2.56

TABLE 2

CDS parameters employed in the simulation

Alloy 1 (pure Al)		Alloy 2 (Al-Si alloy)			Alloy 3 (Al-Si alloy)			ΔT (K)
T_1 (K)	m_1 (kg)	C_2 (wt.%)	T_2 (K)	m_2 (kg)	C_3 (wt.%)	T_3 (K)	T_{L3} (K)	
938.15	1/3	7.2	893.15	2/3	4.8	906.49	904.15	45
		8	888.15		5.3	902.40	901.11	50
		12	858.15		8	883.56	883.15	80
		13	858.15		8.7	879.13	878.26	80
		14.6	888.15		9.7	901.95	871.17	50
		15	893.15		10	906.11	869.01	45

* Fluent 2020R1, Ansys Inc., Pittsburgh, PA, USA
** JMatPro 9.0, Sente Software Corporation, Guildford, UK

2.2. Experiment process

To verify part of the above simulation and calculation results, experiment was conducted. The employed parameters were same to those listed in TABLE 1, only except that the masses of the precursor melts were the twice those in TABLE 2. Correspondingly, the dimensions of the used equipment were also twice those labeled in Fig. 1and the equipment was presented in reference [12]. When 2/3 kg pure Al and 4/3 kg Al-Si alloy were melted in two resistance furnaces at their respective temperatures, they were then simultaneously poured into the third crucible at rates of 1/3 kg and 2/3 kg per second respectively. After mixing, the resultant mixture was immediately poured into a permanent mould with room temperature to form a casting as shown by Fig. 2. It is noted that the temperature of the third crucible was preheated to the liquidus temperature of Alloy 3 prior to mixing. Repeating the above experiment procedure according to the processing parameters listed in TABLE 1, six castings were achieved.

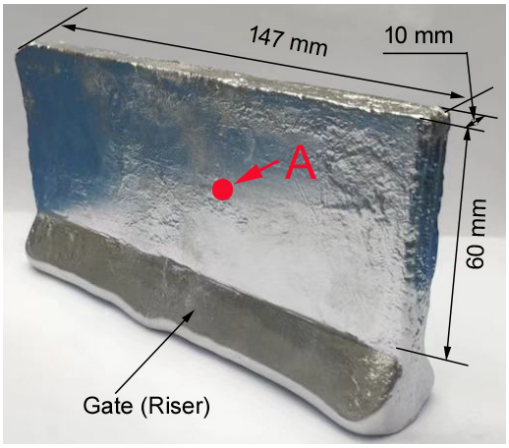

Fig. 2. Photo of the CDS casting

One specimen was cut from the center region of each casting, then finished, polished and etched using Keller's agent (2.5 vol.% HNO_3, 1.5 vol.% HCl, 1 vol.% HF and 95 vol.% distilled water), and finally observed with an Axio Scope A1 optical microscope (OM). The size and shape factor of primary Al grains were examined via Image-Pro Plus 6.0 software*. For each specimen, at least three typical OM images were examined at a magnification of 100 times.

3. Results and discussion

3.1. Simulation and calculation

3.1.1. Effect on temperature and solute fields

Fig. 3 gives the temperature fields in the cross section at half height of the mixtures prepared with different-composition Alloy 2 melts at 0.5 s after mixing (at this time the mixture surface was basically calm). It is found that the temperature field becomes more and more inhomogeneous besides the decrease of general temperature of the mixture as the Si concentration increases to 12% (comparing Fig. 3a-c). As shown by TABLE 1, the employed Alloy 2 temperature continuously decreases as the Si content increases due to the reduction of liquidus temperature. As a result, the difference in temperature between the two precursor melts increases (TABLE 2), leading to the larger temperature difference between the pockets of the two melts in the resultant mixture, and thus, the more inhomogeneous temperature. Of course, the decline of the Alloy 2 temperature must cause the decrease of general temperature in the mixture at the condition that the Alloy 1 temperature keeps at a constant of 938.15 K. However, as the Si content exceeds 12%, the temperature field gets more and more uniform (comparing Fig. d-e). The reason is just opposite to that at the Si content less than 12%. As known, the eutectic composition of Al-Si binary alloy is 12.6% Si [17]. Comparing Fig. 3a with 3f, 3b with 3e, and 3c with 3d, it is seen that the temperature fields at the hypoeutectic compositions are more uniform than those at the corresponding hypereutectic ones when the temperature differences between the precursor melts are same (i.e., when the mixing temperature and liquidus temperature of the hypoeutectic melt are same to those of the hypereutectic melt, TABLE 1). This should be contributed to the larger thermal conductivities of the hypoeutectic alloys than the hypereutectic ones [4]. So it can be concluded that the increase of Si concentration in Alloy 2 within the range of hypoeutectic composition results in the non-homogenization of mixture temperature field, accompanied by a decrease of the general temperature, and opposite results are achieved as the content varies within the hypereutectic range, and the temperatures at the hypoeutectic Alloy 2 melts are more uniform than those at the corresponding hypereutectic ones with the same liquidus and mixing temperatures.

Fig. 4 gives the corresponding solute fields. It should be noted that to show the inhomogeneity of the concentration fields, the scale bars are different for these fields, but their ranges are the same of 0.045, so the composition inhomogeneity for each field can be estimated through comparing the color differences in different regions. Based on this standpoint, it is found that the solute field monotonously becomes more and more inhomogeneous as the Si content increases within the whole employed range from 7.2% to 15%. This is mainly contributed to the increased difference in composition between the two precursor melts caused by the increase in Si content of Alloy 2. In addition, the rise of mixing temperature with the increase of Si content for the hypoeutectic alloys, and the drop in the temperature for the hypereutectic ones, can accelerate and depress the atom diffusion respectively. Furthermore, the resultant enhanced solute gradient between the pockets of the two precursor melts can also expedite the solute diffusion. However, the present result indicates that the crucial factor for determining the solute field is the compositions of the two precursor melts.

In view of the regions marked in Figs. 3a, 3b, 4a and 4b, the temperature and solute fields are quite uniform, but in fact,

* Media Cybernetics, Inc., Rockville, MD, USA

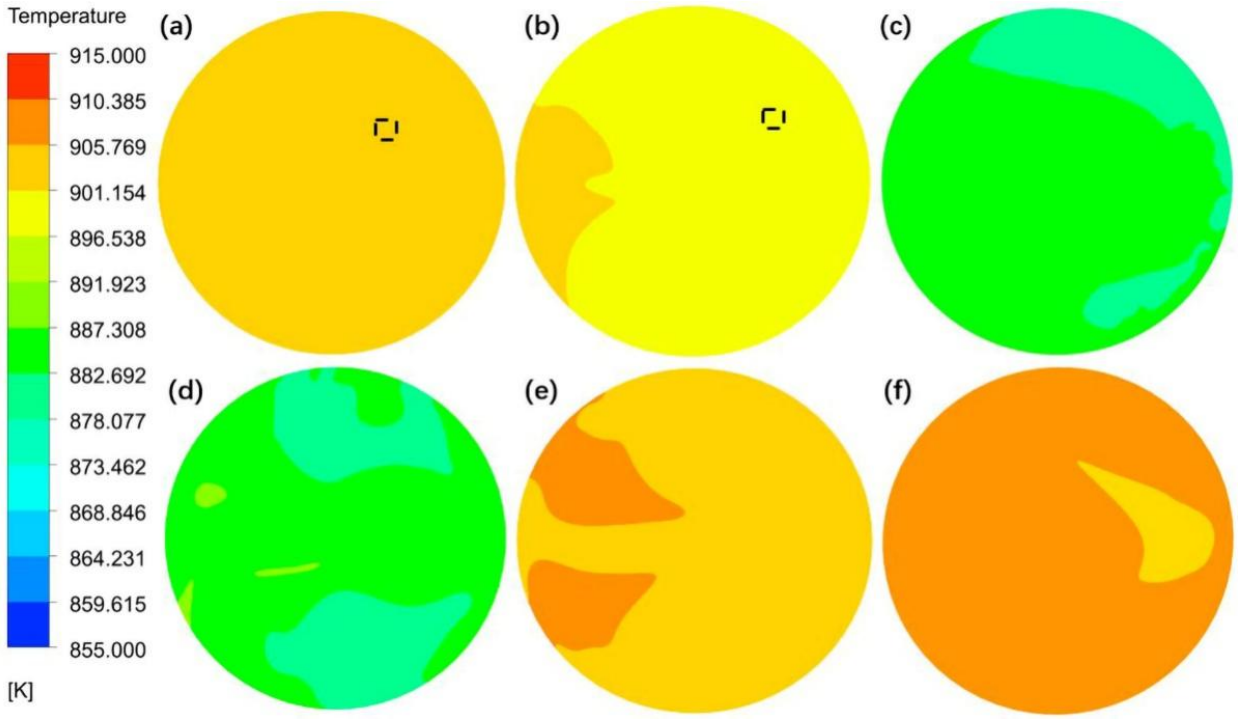

Fig. 3. Temperature fields in the cross section at half height of the mixtures prepared with Alloy 2 melts of (a) Al-7.2Si, (b) Al-8Si, (c) Al-12Si, (d) Al-13Si, (e) Al-14.6Si and (f) Al-15Si

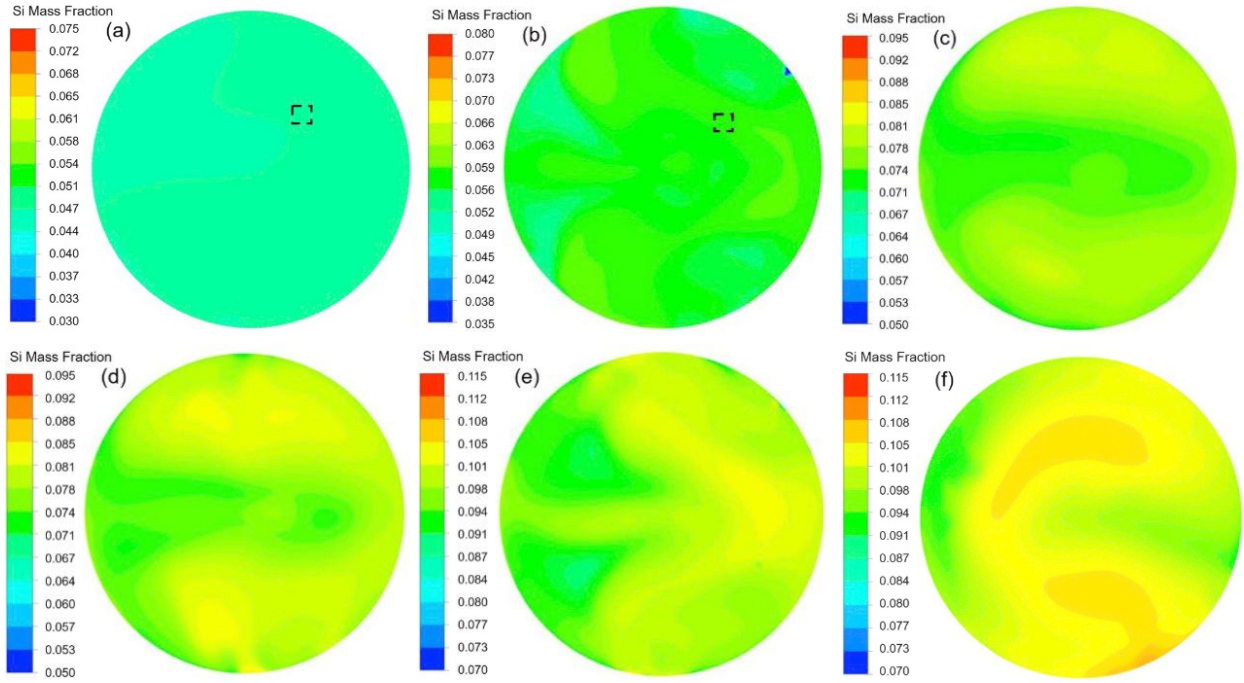

Fig. 4. Solute fields in the cross section at half height of the mixtures prepared with Alloy 2 melts of (a) Al-7.2Si, (b) Al-8Si, (c) Al-12Si, (d) Al-13Si, (e) Al-14.6Si and (f) Al-15Si

both of them are not so uniform as shown by the magnified images in Fig. 5, in which there is an Al-rich pocket (Fig. 5c and d) with high temperature (Fig. 5a and b). In addition, there always has a multilayered transition interface between the Al-rich pocket and surrounding Si-rich melt. As suggested by previous investigation [12,13], these multilayer transition interfaces are composed of numerous fine pockets with different compositions and temperatures, which are originated from the two precursor pockets due to smearing effect at their interfaces. Furthermore, it is seen that the sizes of the Al-rich pockets in the temperature fields are larger than those in the corresponding solute fields (comparing Fig. 5a with 5c, and 5b with 5d). This is ascribed to the larger thermal conductivity than the solute diffusion coefficient [20].

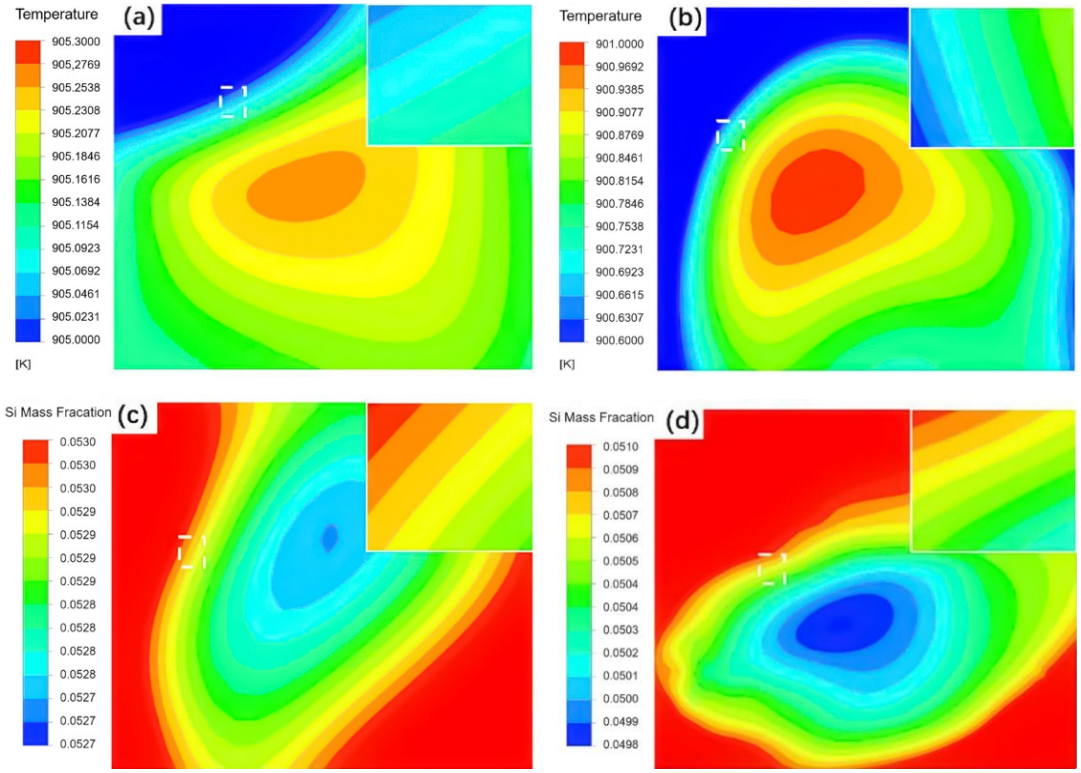

Fig. 5. (a)-(d) Magnified images corresponding to the regions marked in Figs 3(a), 3(b), 4(a) and 4(b) respectively. Inserts are the further magnified images of the regions labelled in (a)-(d

3.1.2. Effect on nucleation rate

Fig. 6 gives the statuses of solidified meshes in the mixtures prepared with the different-composition Alloy 2 melts, in which the red-color meshes refer to the solidified ones while the grey-color meshes represent the liquid ones. It shows that the number of solidified meshes increases as the Si content increases within the hypoeutectic composition (comparing Fig. 6a-c), but then decreases as the concentration exceeds the eutectic point (comparing Fig. 6d-f) and finally decreases to zero at 15% Si (Fig. 6f). This result implies that the nucleation rate is first enhanced as the Si content increases, but then reduced after the content exceeds the eutectic point. The detailed values of solidified mesh percentage are plotted in Fig. 7, which shows

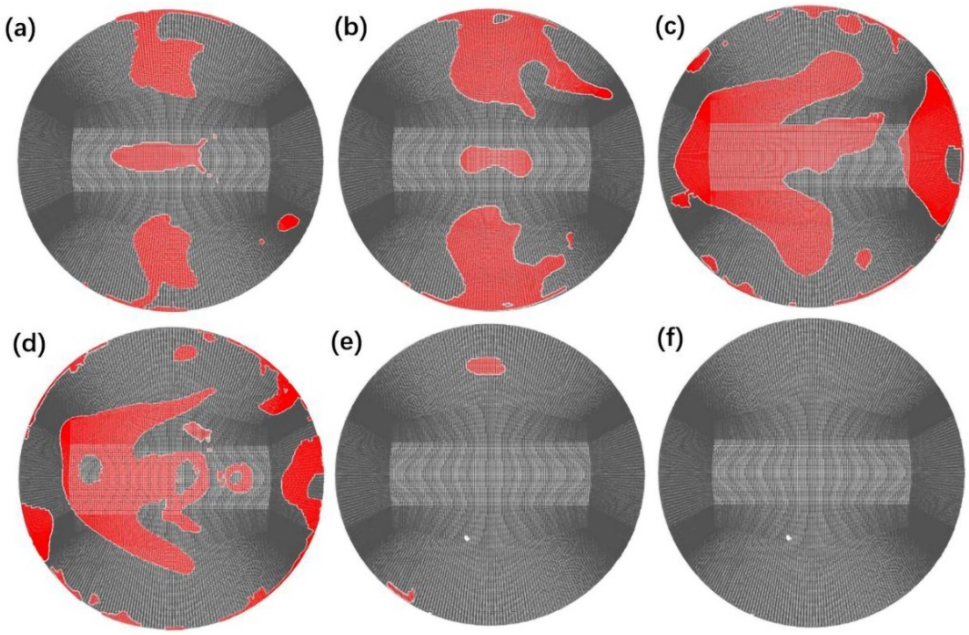

Fig. 6. Schematics of nucleation statuses in the cross section at half height of the mixtures prepared with Alloy 2 melts of (a) Al-7.2Si, (b) Al-8Si, (c) Al-12Si, (d) Al-13Si, (e) Al-14.6Si and (f) Al-15Si. The red-color meshes refer to the solidified ones

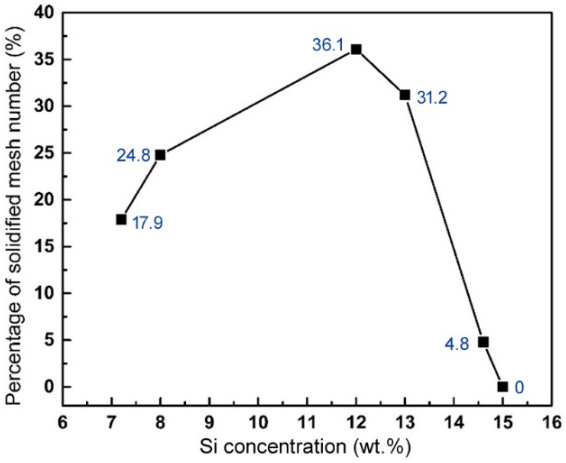

Fig. 7. Variation of percentage of solidified mesh number with Si concentration of Alloy 2

that only the percentages at Si contents of 12% and 13% are higher than 30%. According to a previous investigation from the authors [12], an ideal nondendritic (fine and spheroidal) microstructure can be achieved in the CDS castings only at using these two-composition Alloy 2 melts. It is also found that only the statuses at the two-composition Alloy 2 melts are satisfied with the requirement that the temperature difference between two precursor melts should be higher than 50 K [4].

Fig. 8a as an example gives the calculated interface conditions between pure Al and Al-Si pockets in the mixture prepared using Al-7.2Si melt. It shows that a supercooling zone with width of d and maximum supercooling degree of $\Delta T'$ forms in the Alloy 1 pocket close to the interface of Alloy 1/Alloy 2 pockets, and the other region of the Alloy 1 pocket and the whole Alloy 2 pocket are all in superheat state (the maximum superheats in the Alloy 1 and 2 melts are ΔT_1 and ΔT_2 respectively). As indicated by TABLE 2, what mainly being induced by the increase of Si content in Alloy 2 is the variation of mixing temperature of the Alloy 2 melt. When the Si content increases from 7.2% to 12%, the temperature of Alloy 2 melt falls from 893.15 K to 858.15 K, leading the temperature difference with the Alloy 1 melt to increase from 45 K to 80 K. As a result, the high-temperature (938.15 K) Alloy 1 pockets in the resulted mixture should be cooled to a higher supercooling state ($\Delta T'$) in a wider region (d). But as the content increases within the hypereutectic composition (from 13% to 15%), an opposite result is achieved. The present calculated values are listed in TABLE 3. To clearly show the variations of the two parameters ($\Delta T'$ and d) with the composition of Alloy 2, they were plotted as shown by Fig. 8b. It reveals that both $\Delta T'$ and d continuously increase as the Si content increases from 7.2% to 8%, and then persistently decrease when the content changes from 13% to 15%, which is completely consistent to the above speculations.

As indicated above, the Al-7.2Si and Al-15Si, Al-8Si and Al-14.6Si, and Al-12Si and Al-13Si have the same liquidus temperatures (also the same mixing temperatures), and thus the same temperature differences with the Alloy 1 (pure Al) melt (TABLE 2). So the unique effect of Alloy 2 composition (i.e., the Si content) on the nucleation can be estimated by pairwise comparison of the conditions at these alloys. TABLE 3 and Fig. 8b indicate that both the $\Delta T'$ and d at mixing with the hypoeutectic alloys are all slightly larger than those with the hypereutectic counterparts. It is known that the thermal conductivity of Al-Si alloy decreases with increasing the Si content [17]. Its chilling effect on the Alloy 1 pockets is then decreased and thus, both

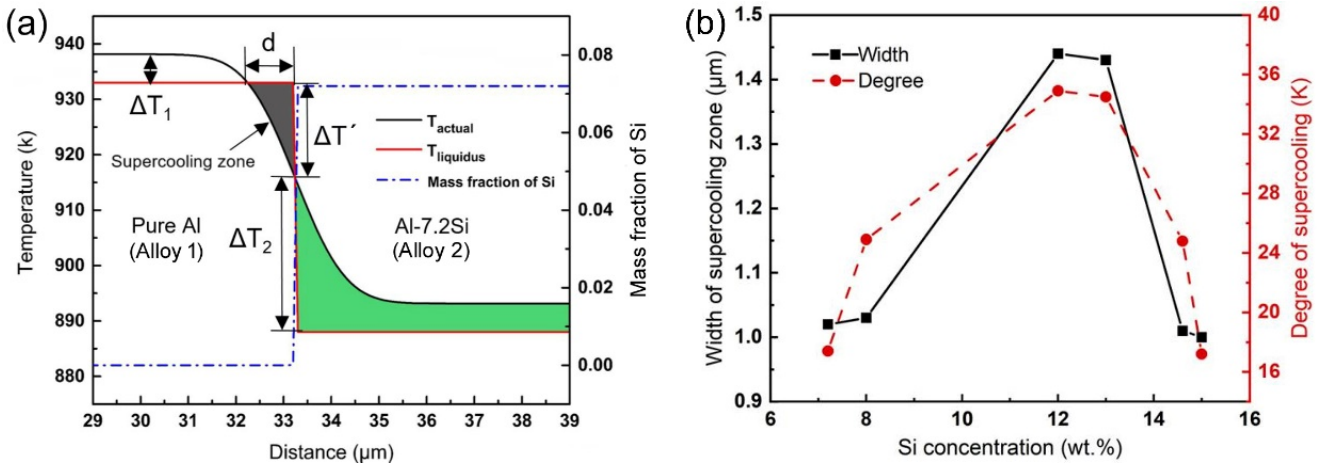

Fig. 8. (a) Interface conditions between pure Al and Al-7.2Si melts, and (b) Variations of supercooling degree and width of supercooling zone in pure Al pocket with Si concentration of Al-Si alloy

TABLE 3

Supercooling degrees ($\Delta T'$) and widths (d) of supercooling zone in pure Al pocket at mixing with different-Si concentration Al-Si melts

Composition of Alloy 2	Al-7.2Si	Al-8Si	Al-12Si	Al-13Si	Al-14.6Si	Al-15Si
Width d (μm)	1.02	1.03	1.44	1.43	1.01	1.00
Degree of supercooling $\Delta T'$ (K)	17.4	24.9	34.9	34.5	24.8	17.2

the $\Delta T'$ and d of the resultant supercooling zone are reduced. However, the Si diffusion in the Alloy 2 melt towards the solid/liquid interface should be accelerated as the Si content increases, due to the increased Si concentration gradient across the interface of Alloy1/Alloy 2 pockets. As a result, the liquidus temperature in the front melt of solid/liquid interface, and thus, the $\Delta T'$ and d, are altered. But the present results reveal that the change in the liquidus temperature resulted from the increase of Si content caused by diffusion is quite little and can be ignored. The reason is contributed to the limited contact time of the two precursor melts during mixing. Therefore, it can be proposed that the effect of the Alloy 2 composition itself with the same liquidus and mixing temperatures (i.e., the same superheating degree and temperature difference with Alloy 1) on the interfacial conditions is very small, but the variation of the mixing temperature of Alloy 2 induced by the change of the liquidus temperature plays a significant effect. As expected, the larger the supercooling degree and the wider the supercooling zone are, the higher the nucleation rate is. Based on this standpoint, the change of the nucleation rate shown in Fig. 7 can be reasonably interpreted. Together with the result about the temperature field discussed above, it can be proposed that the large nonuniformity of the temperature field is beneficial for improving the nucleation rate. The higher nucleation rate should bring about the smaller and more spheroidal primary grains in the resultant castings.

In addition, the superheat degree of the mixture should have large effect on the survival of the early-formed nuclei during mixing, and a high superheat must increase the possibility of the nuclei remelting, being equivalent to the decrease of nucleation rate. As shown by Fig. 9, the superheat degree first slightly decreases from 2.34 K to 0.41 K as the Si content increases within the hypoeutectic range (7.2-12%), and then significantly increases from 0.87 K to 37.1 K after exceeding the eutectic composition (from 13 to 15%). Differing from the relatively symmetrical variations of both the $\Delta T'$ and d as the eutectic composition (Fig. 8b), the change of the superheat degree is very asymmetrical. Besides the drop in mixing temperature of Alloy 2 within the hypoeutectic range and the rise within the hypereutectic range with increasing Si content, the main reason is due to the continuous drop in liquidus temperature of the mixture (Alloy 3), as illustrated in TABLE 2. Therefore, the slight reduction of the superheat degree in the hypoeutectic range and subsequent significant rise in the hypereutectic range are also contributed to the variation of nucleation rate in such way as shown by Fig. 7. It's expected that the higher the superheat degree, the fewer the survived nuclei. That is, the variation of the nucleation rate in such way as shown by Fig. 7 should also be mainly attributed to the change of the superheating degree besides the effects of the supercooling degree and width of supercooling zone. As illustrated by Fig. 7, the survived nuclei are decreased to zero as the Si content increases to 15%. TABLE 2 shows that the temperature difference (45 K) with the Alloy 1 melt is same to that of the Al-7.2Si melt, i.e., like to the mixture with the Al-7.2 Si, nucleation also occurs. But the present result implies that all the formed nuclei rapidly remelt due to the high superheating degree. However, the density of the Alloy 2 melt decreases as the Si content increases because of the smaller density of Si than Al. So the tendency of the Alloy1 melt and the solid phases (i.e., nuclei) that are formed from nucleation in the Alloy 1 melt to sink on the bottom of the mixture should increase as the Si content increases. In this case, the status revealed by Fig. 6f possibly cannot reflect the actual conditions of nucleation. To verify this, the result from a vertical section is presented as shown by Fig. 10, which also indicates that the nucleation rate is zero. When a nucleus forms and does not remelt during subsequent mixing and solidification, it will grow in a planar mode due to no constitutional supercooling zone in the melt ahead of solid/liquid interface in either the Alloy 1 melt side or the Alloy 2 side as shown by Fig. 8a, forming a nondendritic grain.

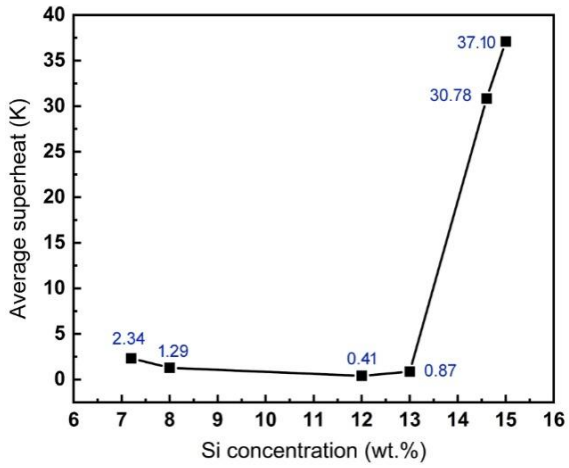

Fig. 9. Variation of average superheat of the mixture with Si concentration in Alloy 2

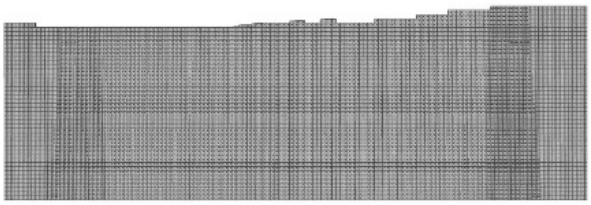

Fig. 10. Schematic of nucleation status in a vertical section of the mixture prepared with the Alloy 2 melt of Al-15Si

As indicated above, one requirement for a successful CDS stipulates that the Gibbs energies of the three melts, the absolute value of sum of two precursor melts' Gibbs energies ($|G_{\max}|$) should be lower than that of Alloy 3 at its liquidus temperature ($|G_{liquidus}|$), i.e., $\Delta G = |G_{\max}| - |G_{liquidus}| < 0$ [15]. The present result indicates that the ΔG first obviously decreases as the Si content increases, and then significantly increases over the eutectic composition, and the conditions at the Si contents ranging from 8% to 13% satisfy the requirement (TABLE 4). So it is proposed that only the castings prepared with these-composition Alloy 2 melts possibly obtain nondendritic microstructure in view of this requirement.

TABLE 4

Absolute values of G_{max} and $G_{liquidus}$, and ΔG ($|G_{max}| - |G_{liquidus}|$) at mixing with different-Si concentration Al-Si melts

Composition of Alloy 2 (wt.%)	Al-7.2Si	Al-8Si	Al-12Si	Al-13Si	Al-14.6Si	Al-15Si
$\|G_{max}\|$ (J)	36292.67	35975.53	34419.23	34240.39	35715.93	35934.65
$\|G_{liquidus}\|$ (J)	36203.96	36033.69	34624.42	34335.86	33673.48	33498.58
ΔG (J)	88.71	–58.16	–205.19	–95.47	2042.45	2436.07

3.2. Experiment

To verify the results from the above simulation and calculation, experiments were conducted and the microstructures of the resultant castings were observed. According to the previous investigations [12,13], the microstructure of the resultant casting is quite uniform, so only the microstructures in the center region of the castings (marked by A in Fig. 2) were presented. As shown by Fig. 11a, the primary α-Al grains in the casting prepared using Al-7.2Si are coarse dendrites. When the Si content in the Alloy 2 melt increases, the dendritic characteristics of the grains gradually disappear, accompanied by significant decrease in size (comparing Fig. 11a-c), and the primary grains become into small and near-spheroidal particles at 12% Si (Fig. 11c).

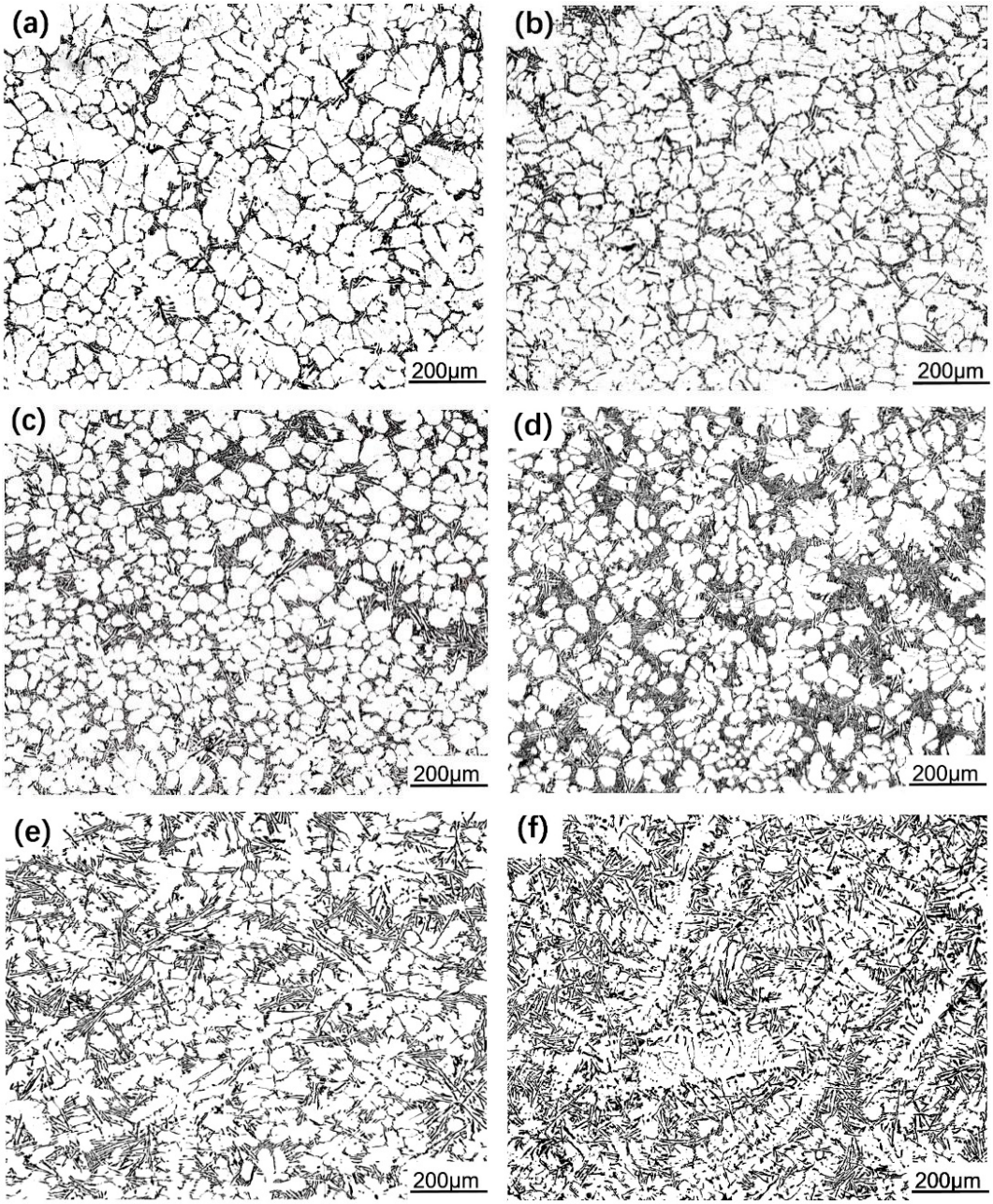

Fig. 11. Microstructures of the CDS castings by using Alloy 2 of (a) Al-7.2Si, (b) Al-8Si, (c) Al-12Si, (d) Al-13Si, (e) Al-14.6Si and (f) Al-15Si

But when the content further increases, i.e., exceeds the eutectic composition, the primary grains then gradually evolve into dendrites (comparing Fig. 11c-e), and completely change into developed dendrites as the content increases to 15% (Fig. 11d). These changes in grain size and morphology can be more clearly seen by the quantitative examination results shown by Fig. 12, which are completely consistent with the results achieved from the above simulation and calculation. In view of the general microstructures, only the castings prepared by Al-12Si and Al-13Si melts have relatively ideal nondendritic microstructure (Fig. 11c and d). This further demonstrates that the percentage of solidified meshes achieved from the simulation must be higher than 30% in order to get an ideal nondendritic microstructure. In addition, the casting prepared using Al-8%Si may also have a nondendritic microstructure in view of the requirement about Gibbs energy as stated above. But the experiment result implies that this requirement is a necessary condition, but not a sufficient condition. The ΔG should be lower than a critical value, for instance, lower than –90 J in the present work.

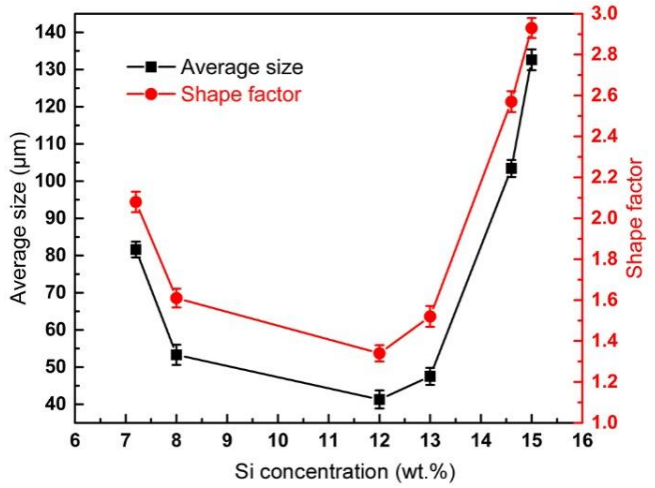

Fig. 12. Variations of size and shape factor of primary grains in the CDS castings with Si concentration in Alloy 2

Fig. 11 also shows that the proportion of primary grains continuously decreases, while that of interdendritic eutectics correspondingly decreases as the Si content increases. This is in accord with the variation in composition of Alloy 3 (i.e., its composition approaches the eutectic point) with increasing the content. Previous investigation proposed that nondendritic grains could only be originated from the Alloy 1 pockets in the mixture, because the solidification behavior of the Alloy 2 melt was identical to the traditional one, always forming a dendritic structure [21,22]. According to this proposal, the mass of Alloy 1 should not be too small. This should be the main reason that the requirement claims that the mass ratio of Alloy1/Alloy 2 is not lower than 3:1 besides achieving a good mixing effect [17]. But the present result indicates that not all of Alloy 1 melt transforms into primary grains during CDS even if it is a pure metal, and the proportion of primary grains is closely related to the composition of target alloy, although the solidification during CDS is more non-equilibrated than that of traditional solidification due to the deliberately caused composition inhomogeneities during mixing [19]. This proportion not only is depended on the compositions of two precursor melts, but also is determined by the composition homogenization between two precursor melt pockets resulted from diffusion. For an ideal CDS microstructure, it should be composed of small spheroidal primary grains and intergranular eutectics. To achieve such a microstructure, the composition of Alloy 1 should be close to pure metal while that of Alloy 2 should approach to eutectic composition. In addition, the resultant mixture should be cast as soon as possible to reduce the composition homogenization caused by diffusion.

4. Conclusions

(1) At a given superheat, the increase of Si content in Al-Si alloy (Alloy 2) within the hypoeutectic composition range lowers the liquidus temperature, i.e., decreases the mixing temperature of the Al-Si alloy (Alloy 2), and thus, increases the temperature difference with pure Al (Alloy 1), leading the temperature field of the resulted mixture (Alloy 3) to become more inhomogeneous. As the Si content increases within the hypereutectic composition range, an opposite result is achieved due to the inverse cause. But for the solute field of the mixture (Alloy 3), it always becomes more inhomogeneous due to the continuously increased composition difference between the two precursor melts.

(2) At a same liquidus temperature, the temperature field of the mixture prepared using hypoeutectic Al-Si alloy is more slightly uniform than that prepared using hypereutectic one due to the higher thermal conductivity of the hypoeutectic alloy.

(3) The achieved supercooling degree and width of supercooling zone in the pure Al pockets first increases as the Si content increases within the hypoeutectic composition range, and then decreases within the hypereutectic range due to the same reason as the effect on the temperature field. Similarly, these two parameters at employing a hypoeutectic alloy are slightly larger than that at utilizing a hypereutectic one with the same liquidus temperature as the hypoeutectic alloy.

(4) The larger the supercooling degree and width of supercooling zone, and the higher the nucleation rate, and thus, the smaller and more spheroidal of the primary α-Al grains in the CDS casting, and vice versa. But the nucleation rate at using a hypoeutectic alloy is always significantly higher than that at utilizing a hypereutectic alloy when they have a same liquidus temperature, because of the significant rise of the mixture superheat.

(5) The requirement about the Gibbs energies of the three melts proposed in previous investigations is a necessary condition, but not a sufficient condition for a successful CDS.

(6) The experiment results about the variations of primary α-Al size and morphology are consistent to the results deduced

from the simulation and calculation. The present results further demonstrate that an ideal nondendritic casting can be obtained only when the percentage of solidified meshes is up to 30%. Similar to the traditional solidification, the proportion of primary α-Al grains continuously decreases as Alloy 3 composition approaches its eutectic composition (i.e., the Si content in Alloy 2 increases).

Acknowledgement

This work was supported by the National Key Research and Development Program of China (grant number 2018YFB2001800).

REFERENCES

[1] M. Lalpoor, D.G. Eskin, L. Katgerman, Fracture behavior and mechanical properties of high strength aluminum alloys in the as-cast condition. Mater. Sci. Eng. A. **497** (1-2), 186-194 (2008). DOI: https://doi.org/10.1016/j.msea.2008.06.047

[2] D. Saha, S. Shankar, D. Apelian, M. Makhlouf, Casting of aluminum-based wrought alloys using controlled diffusion solidification. Metall. Mater. Trans. **35A** (7), 2174-2180 (2004). DOI: https://doi.org/10.1007/s11661-004-0167-8

[3] Z. Fan, X. Fang, S. Ji, Microstructure and mechanical properties of rheo-diecast (RDC) aluminium alloys. Mater. Sci. Eng. A. **412** (1-2), 298-306 (2005). DOI: https://doi.org/10.1016/j.msea.2005.09.001

[4] A.A. Khalaf, Controlled diffusion solidification: Process mechanism and parameter study. PhD thesis, McMaster University, Hamilton 2010.

[5] R. Ghiaasiaan, X. Zeng, S. Shankar, Controlled diffusion solidification (CDS) of Al-Zn-Mg-Cu (7050): Microstructure, heat treatment and mechanical properties. Mater. Sci. Eng. A. **594**, 260-277 (2014). DOI: http://doi.org/10.1016/j.msea.2013.11.087

[6] X. Yang, Y.D. Li, X.M. Luo, Microstructural evaluation and mechanical properties of 7075 aluminum alloy prepared by controlled diffusion solidification. China Foundry **16** (4), 238-247 (2019). DOI: https://doi.org/10.1007/s41230-019-9059-9

[7] R. Ghiaasiaan, S. Shankar, Microstructure, intermetallic phases, and fractography of the cast Al-5.8Zn-2.2Mg-2.5Cu alloy by controlled diffusion solidification. Metall. Mater. Trans. A. **51** (9), 4711-4726 (2020). DOI: https://doi.org/10.1007/s11661-020-05885-z

[8] M. Pourgharibshahi, M. Divandari, H.S. Larijani, P. Ashtari, Controlled diffusion solidification processing: A review. J. Mater. Process. Technol. **250**, 203-219 (2017). DOI: https://doi.org/10.1016/j.jmatprotec.2017.07.018

[9] A.A. Khalaf, S. Shankar, Mechanism of anomalous grain formation during controlled diffusion solidification. JOM **72** (11), 3733-3743 (2020). DOI: https://doi.org/10.1007/s11837-020-04198-1

[10] A.A. Khalaf, S. Shankar, Effect of mixing rate on the morphology of primary Al phase in the controlled diffusion solidification (CDS) process. J. Mater. Sci. **47** (23), 8153-8166 (2012). DOI: https://doi.org/10.1007/s10853-012-6711-9

[11] Y.D. Li, X.L. Zang, Y. Ma, D. Apelian, H.W. Zhou, Effect of mixing rate and temperature on primary Si phase of hypereutectic Al-20Si alloy during controlled diffusion solidification (CDS) process. China Foundry. **12** (3), 173-179 (2015).

[12] T.J. Chen, X.K. Yang, H. Xue, G.L. Bi, X.Z. Zhang, R.G. Guan, Mixing process and nucleation of an Al-Si alloy during controlled diffusion solidification with simultaneous mixing and effect of mixing rate. J. Mater. Sci. **57** (4), 3018-3040 (2022). DOI: https://doi.org/10.1007/s10853-021-06730-3

[13] Y.H. Liu, T.J. Chen, Effect of standing time after mixing on the mixture microstructure of an Al-Si alloy during controlled diffusion solidification with simultaneous mixing. Metals **13**, 733 (2023). DOI: https://doi.org/10.3390/met13040733

[14] H. Xue, T. Chen, X. Zhang, G. Bi, Y. Ma, R. Guan, Effect of mixing temperature on microstructure of an Al-Si alloy prepared by controlled diffusion solidification. China Foundry **20**, 241-252 (2023). DOI: https://doi.org/10.1007/s41230-023-2067-9

[15] D. Apelian, M.M. Makhlouf, D. Saha, CDS method for casting aluminium-based wrought alloy compositions: Theoretical framework. Mater. Sci. Forum. **519-521**, 1771-1776 (2006). DOI: https://doi.org/10.4028/www.scientific.net/msf.519-521.1771

[16] E. Cini, B. Vinet, P.J. Desre, A thermodynamic approach to homogeneous nucleation via fluctuations of concentration in binary liquid alloys. Philos. Mag. A. **80** (4), 955-966 (2000). DOI: https://doi.org/10.1080/01418610008212092

[17] A.A. Khalaf, Microstructure evolution of Al-Si hypoeutectic alloys prepared by controlled diffusion solidification. Int. J. Adv. Manuf. Tech. **120**, 5003-5014 (2022). DOI: https://doi.org/10.1007/s00170-022-09075-6.

[18] R. Ghiaasiaan, S. Shankar, Effect of alloy composition on microstructure and tensile properties of net-shaped castings of Al-Zn-Mg-Cu alloys. Int. J. Metalcasting **13** (2), 300-310 (2019). DOI: https://doi.org/10.1007/s40962-018-0254-z

[19] A.A. Khalaf, S. Shankar, Favorable environment for a nondendritic morphology in controlled diffusion solidification. Metall. Mater. Trans. A. **42A** (8), 2456-2465 (2011). DOI: https://doi.org/10. 1007/s11661-011-0641-z

[20] S. Ji, Z. Fan. Solidification behavior of Sn-15 Wt Pct Pb alloy under a high shear rate and high intensity of turbulence during semisolid processing. Metall. Mater. Tran. A **33**, 3511-3520 (2002). DOI: https://doi.org/10.1007/s11661-002-0338-4

[21] A.A. Khalaf, Mechanism of controlled diffusion solidification: Mixing, nucleation and growth. Acta. Mater. **103**, 301-310 (2016). DOI: https://doi.org/10.1016/j.actamat.2015.10.011

[22] A.A. Khalaf, Studying of non-dendritic microstructure forming in controlled diffusion solidification. Int. J. Met. **16** (1), 223-233 (2022). DOI: https://doi.org/10.1007/s40962-021-00590-y